The following Communications have been judged by at least two referees to be “very important papers” and will be published online at www.angewandte.org soon:

*K. W. Eberhardt, C. L. Degen, A. Hunkeler, B. H. Meier**
One- and Two-Dimensional NMR Spectroscopy with a Magnetic-Resonance Force Microscope

*S. Wan, J. Guo, J. Kim, H. Ihee, D. Jiang**
A Belt-Shaped, Blue-Luminescent and Semiconducting Covalent Organic Framework

*J. Steill, J. Zhao, C.-K. Siu, Y. Ke, U. H. Verkerk, J. Oomens, R. C. Dunbar, A. C. Hopkinson, K. M. Siu**
Structure of the Observable Histidine Radical Cation in the Gas Phase: a Captodative α-Radical Ion

*Z. Deng, I. Bald, E. Illenberger, M. A. Huels**
Bond- and Energy-Selective Carbon Abstraction from D-Ribose by Hyperthermal Nitrogen Ions

*J. Spielmann, F. Buch, S. Harder**
Early Main-Group Metal Catalysts for the Hydrogenation of Alkenes with Hydrogen

C. Schäffer, A. Merca, H. Bögge, A. M. Todea, M. L. Kistler, T. Liu, R. Thouvenot, P. Gouzerh, A. Müller**
Unprecedented and Differently Applicable Pentagonal Units in a Dynamic Library: A Keplerate of the Type $\{(W)W_5\}_{12}\{Mo_2\}_{30}$

*T. Seiser, N. Cramer**
Enantioselective C–C Bond Activation of Allenylcyclobutanes: Access to Cyclohexenones with Quaternary Stereogenic Centers

*S. W. Hong, M. Byun, Z. Lin**
Robust Self-Assembly of Highly Ordered Complex Structures by Controlled Evaporation of Confined Microfluids

News

Obituary

Books

Highlights

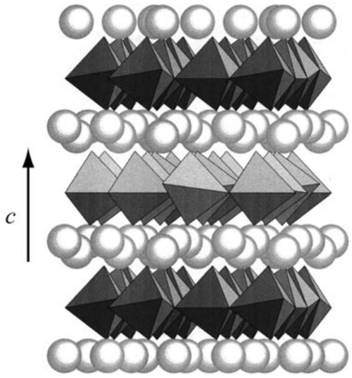

A ferroic performance: In crystals with both electric and magnetic order, a coupling between the orderings may exist: An applied electric field induces a change of magnetization and an applied magnetic field induces a change of polarization. This magnetoelectric effect makes so-called multiferroics potential future information technology devices in which data can be written to magnetic memory elements by applied electric fields.

Multiferroics

Contents

Nanomotors

M. Burghard* ______ 8565 – 8566

A Freight Train of Nanotubes for Cargo Transport on the Nanoscale

An electrically driven nanomotor comprising a short nanotube sheath on a coaxial nanotube axis has been constructed in a further step in the development of rotors based on carbon nanotubes. A current flowing through the axis generates a temperature gradient, which propels the loaded sheath forward a distance in the subnanometer region (see picture).

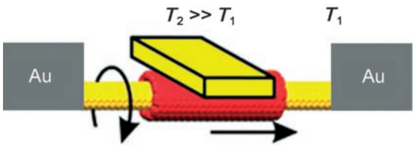

Minireviews

Magnetic Resonance Imaging

E. J. Werner, A. Datta, C. J. Jocher, K. N. Raymond* ______ 8568 – 8580

High-Relaxivity MRI Contrast Agents: Where Coordination Chemistry Meets Medical Imaging

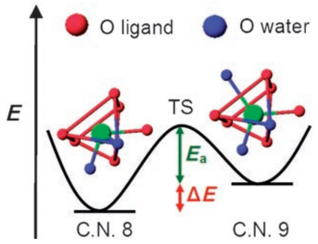

The unique electronic properties of Gd^{III} make it ideal for use in contrast agents for magnetic resonance imaging, but toxic Gd^{III} must be complexed before administration. Designing ligands to form stable complexes while keeping the hydration number high and the water exchange rate optimal remains a challenge. Complexes of hydroxypyridinone chelates combine all the favorable properties for the high relaxivities required in high-field-strength applications.

Reviews

Immobilized Proteins

S. Hudson,* J. Cooney, E. Magner* ______ 8582 – 8594

Proteins in Mesoporous Silicates

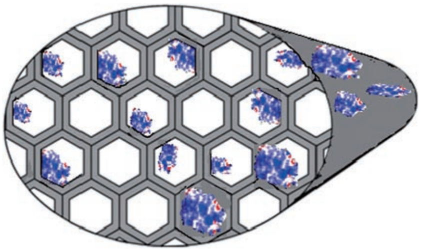

Inner beauty: Since the discovery of mesoporous silicates, novel syntheses have led to precise control over their pore size and structure, particle size, chemical composition, and stability, allowing the adsorption of a wide variety of biological macromolecules. This Review discusses the development of ordered, large-pore, functionalized mesoporous silicates and their application to the immobilization of proteins for biocatalysis.

Communications

Functional Patterning

M. Cavallini,* I. Bergenti, S. Milita, G. Ruani, I. Salitros, Z.-R. Qu, R. Chandrasekar, M. Ruben* ______ 8596 – 8600

Micro- and Nanopatterning of Spin-Transition Compounds into Logical Structures

Changing stripes: The spin-transition compound **1** can be nanopatterned by unconventional and soft lithography to give crystalline, well-oriented, µm-scale structures arranged in stripes on a silica surface. These findings have potential applications in electronic devices and information storage.

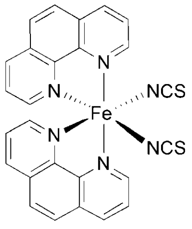

1

For the USA and Canada: ANGEWANDTE CHEMIE International Edition (ISSN 1433-7851) is published weekly by Wiley-VCH, PO Box 191161, 69451 Weinheim, Germany. Air freight and mailing in the USA by Publications Expediting Inc., 200 Meacham Ave., Elmont, NY 11003. Periodicals postage paid at Jamaica, NY 11431. US POSTMASTER: send address changes to *Angewandte Chemie*, Wiley-VCH, 111 River Street, Hoboken, NJ 07030. Annual subscription price for institutions: US$ 7225/6568 (valid for print and electronic / print or electronic delivery); for individuals who are personal members of a national chemical society prices are available on request. Postage and handling charges included. All prices are subject to local VAT/sales tax.

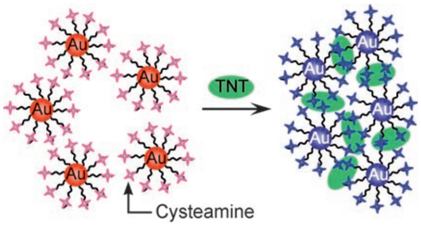

An explosive situation: By using gold nanoparticles and taking advantage of the donor–acceptor interaction between trinitrotoluene (TNT) and cysteamine, the visualization of TNT can be achieved at picomolar levels (see picture). The color change from red to blue can be seen with the naked eye, which allows sensitive on-the-spot detection.

TNT Sensor

Y. Jiang, H. Zhao, N. Zhu, Y. Lin, P. Yu, L. Mao* ________ **8601 – 8604**

A Simple Assay for Direct Colorimetric Visualization of Trinitrotoluene at Picomolar Levels Using Gold Nanoparticles

---

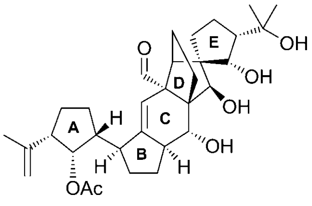

“vannusal B”

The truth is out there: The chase for the originally assigned structure of vannusal B (see structural formula) by total synthesis ended successfully, but created a new puzzle, that of the true structure of this intriguing marine natural product.

Natural Products

K. C. Nicolaou,* H. Zhang, A. Ortiz, P. Dagneau ________ **8605 – 8610**

Total Synthesis of the Originally Assigned Structure of Vannusal B

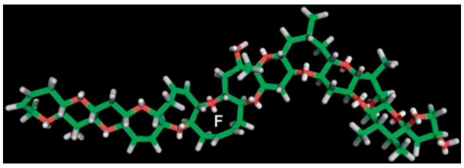

Playing a central role: Ciguatoxins, potent neurotoxins, span a length of over 3 nm and consist of 13 fused ether rings (from the A to the M ring; see energy-minimized structure). The finding that two fully synthetic F-ring-modified analogues have markedly diminished biological activities demonstrates that the central F ring plays a major role in organizing the ciguatoxin molecule into a shape suitable for bioactivity.

Structure–Activity Relationships

VIP

M. Inoue,* N. Lee, K. Miyazaki, T. Usuki, S. Matsuoka, M. Hirama* __ **8611 – 8614**

Critical Importance of the Nine-Membered F Ring of Ciguatoxin for Potent Bioactivity: Total Synthesis and Biological Evaluation of F-Ring-Modified Analogues

---

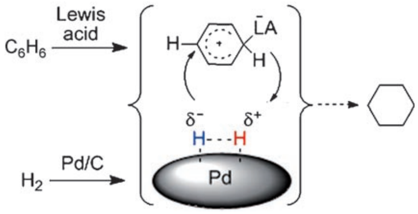

Tackling aromaticity: The title reaction was accomplished by simultaneous activation of molecular hydrogen and the aromatic substrate by Pd/C and a Lewis acidic ionic liquid, respectively. Even benzene and C_{60} fullerene were hydrogenated under ambient conditions (1 bar of H_2 at room temperature). An ionic hydrogenation mechanism (see scheme) is supported by characterization of a stabilized arenium intermediate.

Catalysis

R. R. Deshmukh, J. W. Lee, U. S. Shin,* J. Y. Lee, C. E. Song* ________ **8615 – 8617**

Hydrogenation of Arenes by Dual Activation: Reduction of Substrates Ranging from Benzene to C_{60} Fullerene under Ambient Conditions

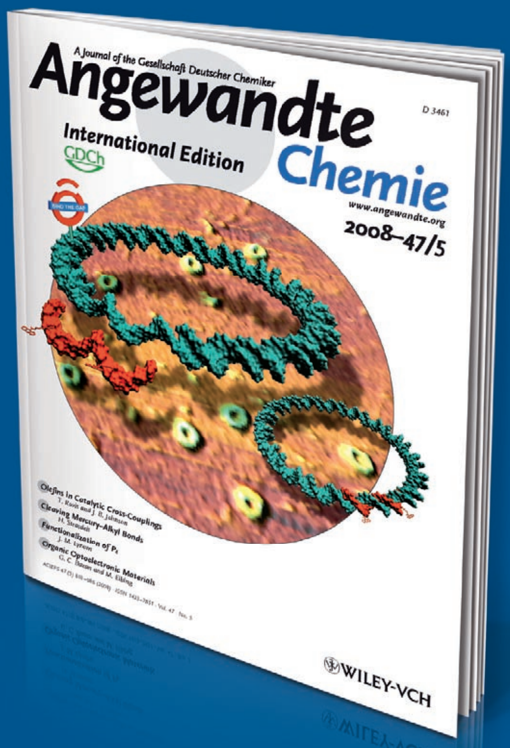
A Journal of the Gesellschaft Deutscher Chemiker
Angewandte Chemie
International Edition
GDCh
D 3461
www.angewandte.org
2008–47/5
WILEY-VCH

Thermoelectricity

J. R. Sootsman, H. Kong, C. Uher,
J. J. D'Angelo, C.-I. Wu, T. P. Hogan,
T. Caillat, M. G. Kanatzidis* **8618 – 8622**

Large Enhancements in the Thermoelectric Power Factor of Bulk PbTe at High Temperature by Synergistic Nanostructuring

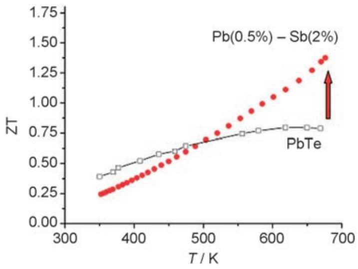

Co-nanostructuring of PbTe with two kinds of metallic nanoparticles (Pb and Sb) can significantly increase its power factor at high temperatures (up to 87% at 700 K; see picture, ZT = figure of merit). The electrical conductivity is dramatically increased at high temperatures without degrading the thermopower. This emergent synergy results only when both Pb and Sb nanocrystals are present.

Chiral Microporous Materials

M.-L. Feng, D.-N. Kong, Z.-L. Xie,
X.-Y. Huang* ______ **8623 – 8626**

Three-Dimensional Chiral Microporous Germanium Antimony Sulfide with Ion-Exchange Properties

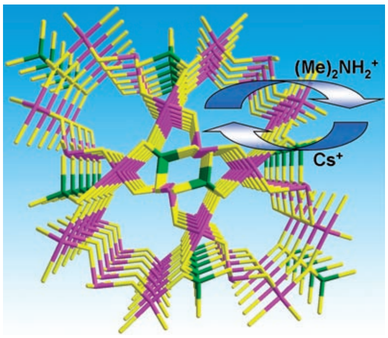

Chiral hole: The first chiral microporous germanium antimony sulfide with 3D helical channels was constructed by the unprecedented combination of $\{GeS_4\}$ tetrahedra and ψ-$\{SbS_4\}$ trigonal bipyramids. The dimethylammonium cations present in the structure are easily exchanged with alkali metal cations present in aqueous solution. The title compound has high ion-exchange capacity and high selectivity for Cs^+ ions.

Protein Microarrays

M.-L. Chen, A. K. Adak, N.-C. Yeh,
W.-B. Yang, Y.-J. Chuang, C.-H. Wong,
K.-C. Hwang, J.-R. R. Hwu, S.-L. Hsieh,
C.-C. Lin* ______ **8627 – 8630**

Fabrication of an Oriented Fc-Fused Lectin Microarray through Boronate Formation

A stable, covalent, and highly active protein microarray was created through the formation of cyclic esters between surface boronic acids and the carbohydrate moiety of a fusion protein, Fc-dectin-1 (see picture). A biotin-labeled polysaccharide was used as a probe to investigate the binding activity of the protein. Staining of the product array with streptavidin-Cy3 revealed the effectiveness of this immobilization strategy.

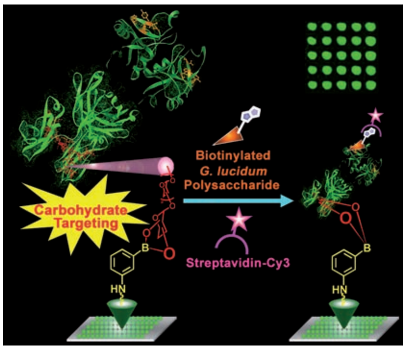

High Oxidation States

P. Hrobárik,* M. Kaupp,*
S. Riedel ______ **8631 – 8633**

Is Allred's $[Hg(cyclam)]^{3+}$ a True Mercury(III) Complex?

Relativistic density functional calculations are used to examine the spectroscopic parameters of $[Hg(cyclam)]^{3+}$ (cyclam = 1,4,8,11-tetraazacyclotetradecane; see picture), which is thought to contain Hg^{3+}, and to analyze its electronic structure. Although the computed EPR parameters and excitation energies are consistent with the experimental data, a detailed analysis of the electronic structure contradicts the assignment as an Hg^{III} complex.

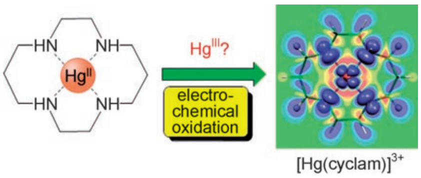

Hybrid Materials

A. J. Bailey, C. Lee, R. K. Feller, J. B. Orton,
C. Mellot-Draznieks, B. Slater,
W. T. A. Harrison, P. Simoncic,
A. Navrotsky, M. C. Grossel,
A. K. Cheetham* ———— **8634–8637**

Comparison of Chiral and Racemic Forms of Zinc Cyclohexane *trans*-1,2-Dicarboxylate Frameworks: A Structural, Computational, and Calorimetric Study

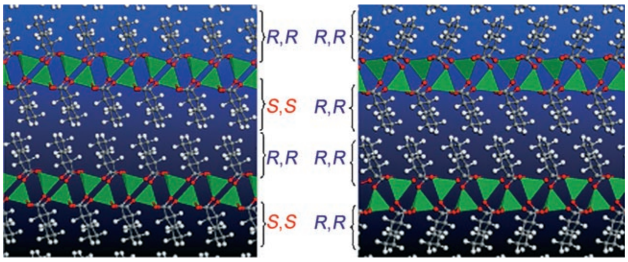

An integrated study of the organic–inorganic framework material zinc cyclohexane *trans*-1,2-dicarboxylate involving synthesis, structure elucidation, computer simulation, and calorimetry shows that the chiral *R*,*R* form (right in picture) is less stable than its racemic *R*,*R*/*S*,*S* analogue (left) and adopts a layered structure with a fundamentally different topology. The results point to the possibility that the structural diversity of racemic frameworks and their homochiral analogues may be much greater than has hitherto been suspected.

CdSe Nanocrystals

O. Chen, X. Chen, Y. Yang, J. Lynch, H. Wu,
J. Zhuang, Y. C. Cao* ———— **8638–8641**

Synthesis of Metal–Selenide Nanocrystals Using Selenium Dioxide as the Selenium Precursor

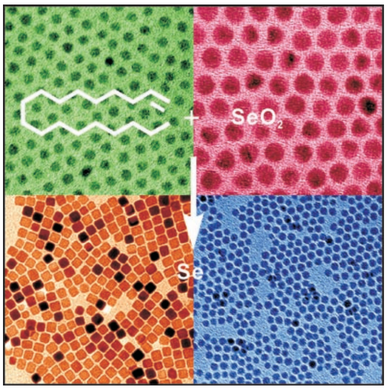

Quality and quantity: A non-injection synthesis of high-quality CdSe nanocrystals can be conducted in air, that is without the need for any oxygen-free manipulation. The synthesis, which uses SeO$_2$ as the selenium precursor, is suitable for the large-scale industrial synthesis of high-quality nanocrystals at low cost and has been generalized for the formation of other metal selenides, such as PbSe and Pd$_{4.5}$Se nanocrystals.

Fullerenes

X. Lu, H. Nikawa, T. Tsuchiya, Y. Maeda,
M. O. Ishitsuka, T. Akasaka,* M. Toki,
H. Sawa, Z. Slanina, N. Mizorogi,
S. Nagase* ———— **8642–8645**

Bis-Carbene Adducts of Non-IPR La$_2$@C$_{72}$: Localization of High Reactivity around Fused Pentagons and Electrochemical Properties

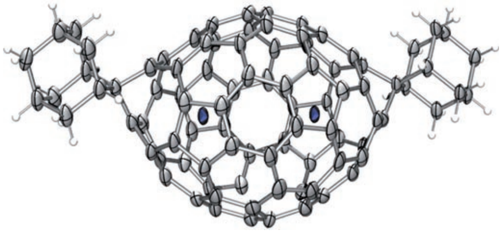

Candylike fullerene: Two adamantylidene (Ad) groups are covalently bonded to the two fused-pentagon sites of the non-IPR endohedral metallofullerene La$_2$@C$_{72}$ in bis-adduct La$_2$@C$_{72}$Ad$_2$. Its open-cage structure, reminiscent of a wrapped candy, was determined by single-crystal X-ray diffraction (see picture), and it retains the electronic structure of pristine La$_2$@C$_{72}$.

Mass Spectrometry

Y. Xia, Z. Ouyang,
R. G. Cooks* ———— **8646–8649**

Peptide Fragmentation Assisted by Surfaces Treated with a Low-Temperature Plasma in NanoESI

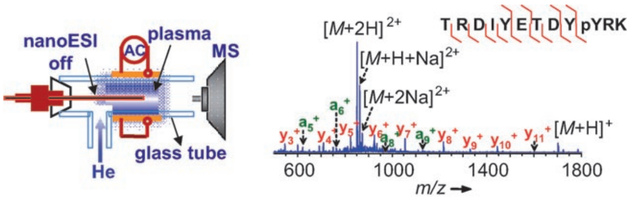

A softy toughens up: When a nanoelectrospray (nanoESI) emitter was exposed first to a helium plasma (see illustration of experimental setup), ESI, a widely accepted “soft” ionization technique, caused significant and useful peptide fragmentation. The appearance of abundant peptide-fragment ions in the mass spectrum was ascribed to electrolyte release into the solution. Labile phosphate groups on the peptide were preserved during fragmentation.

Subcolloidal zeolite particles having all the structural features of the zeolite framework but sizes of only a few unit cells which are insufficient to generate a diffraction pattern exist in silicalite-1 synthesis solutions, as revealed by synchrotron-based reflection–absorption IR spectroscopy on zeolite films prepared from clear precursor solutions by the Langmuir–Blodgett method or by spin coating (see picture).

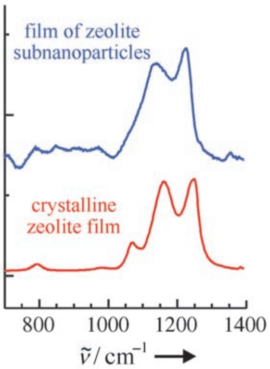

Zeolite Subnanoparticles

L. Tosheva,* B. Mihailova, L. H. Wee, B. Gasharova, K. Garbev, A. M. Doyle* ______ 8650 – 8653

Indirect Observation of Structured Incipient Zeolite Nanoparticles in Clear Precursor Solutions

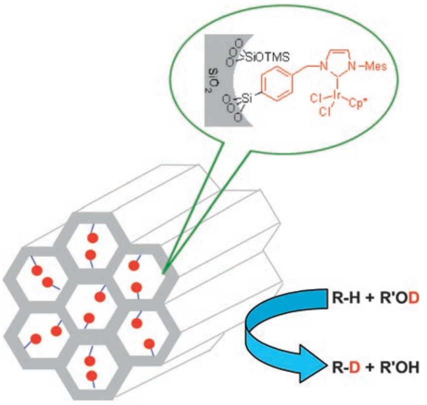

A tailored hybrid mesostructured material containing regularly distributed imidazolium units, and subsequent transformation of these imidazolium moieties into Ir-NHC (NHC = N-heterocyclic carbene) complexes via the formation of Ag-NHC species in situ and further transmetalation with $[\{IrCp^*Cl_2\}_2]$, gives a well-defined, active, and reusable Ir-NHC heterogeneous catalyst for H/D exchange reactions (see picture).

Catalytic Hybrid Materials

T. K. Maishal, J. Alauzun, J.-M. Basset, C. Copéret, R. J. P. Corriu,* E. Jeanneau, A. Mehdi, C. Reyé, L. Veyre, C. Thieuleux* ______ 8654 – 8656

A Tailored Organometallic–Inorganic Hybrid Mesostructured Material: A Route to a Well-Defined, Active, and Reusable Heterogeneous Iridium NHC Catalyst for H/D Exchange

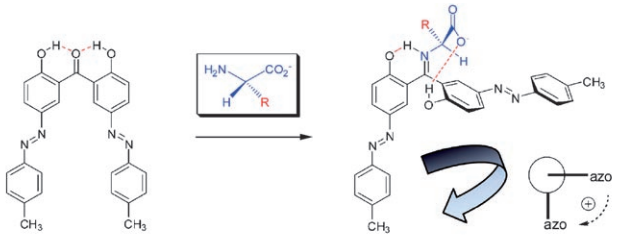

Helical chirality can be imprinted onto a 2,2′-dihydroxybenzophenone derivative (see picture) in a highly stereospecific manner. A single amino acid combines with the receptor to form an imine with two internal hydrogen bonds. The azo group allows sensing of amino acid enantiopurity by circular dichroism spectroscopy.

Chirality Sensors

H. Kim, S. M. So, C. P.-H. Yen, E. Vinhato, A. J. Lough, J.-I. Hong,* H.-J. Kim,* J. Chin* ______ 8657 – 8660

Highly Stereospecific Generation of Helical Chirality by Imprinting with Amino Acids: A Universal Sensor for Amino Acid Enantiopurity

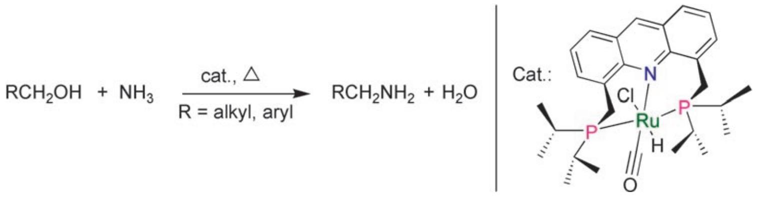
$$RCH_2OH + NH_3 \xrightarrow[R\,=\,\text{alkyl, aryl}]{\text{cat., }\Delta} RCH_2NH_2 + H_2O$$

Air stable and waterproof: Selective and efficient synthesis of primary amines directly from alcohols and ammonia is achieved under mild conditions (see scheme). The reaction is homogenously catalyzed by a novel air-stable ruthenium pincer complex and can proceed in toluene or even in the absence of solvent or "on water".

Homogeneous Catalysis

C. Gunanathan, D. Milstein* ______ 8661 – 8664

Selective Synthesis of Primary Amines Directly from Alcohols and Ammonia

Microgels

M. Serrano Ruiz, A. Romerosa,*
B. Sierra-Martin,
A. Fernandez-Barbero ______ **8665 – 8669**

A Water Soluble Diruthenium–Gold Organometallic Microgel

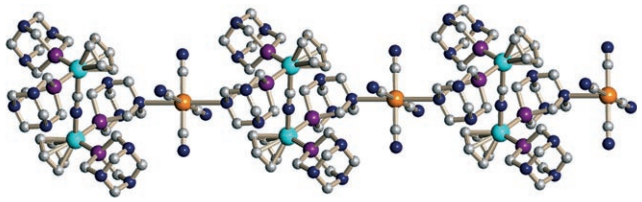

Bridging the gap: Two metal-containing moieties, $[CpRuCNRuCp]^+$ and $[Au(CN)_4]^-$, are bridged through a pta ligand in the P,N coordination mode in a water-soluble, air-stable heterobimetallic coordination polymer (see picture, Au orange, Ru turquoise, C gray, N blue, P purple). This complex exhibits gel-like behavior in water, specifically a thermally controlled volume transition. pta = 1,3,5-triaza-7-phosphaadamantane, Cp = cyclopentadienyl.

Asymmetric Catalysis

L. J. Wang, X. H. Liu, Z. H. Dong, X. Fu,
X. M. Feng* ______ **8670 – 8673**

Asymmetric Intramolecular Oxa-Michael Addition of Activated α,β-Unsaturated Ketones Catalyzed by a Chiral *N*,*N*′-Dioxide Nickel(II) Complex: Highly Enantioselective Synthesis of Flavanones

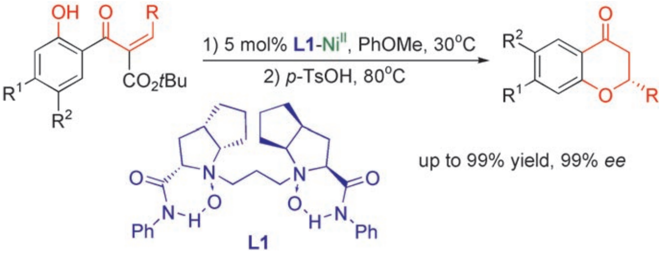

The title reaction provides a promising approach for the synthesis of chiral flavanones with broad substrate scope and is tolerant to air and moisture. Good to excellent enantioselectivities and high yields were achieved for most substrates under mild conditions.

Phosphorus Heterocycles

D. A. Smith, A. S. Batsanov, K. Miqueu,
J.-M. Sotiropoulos, D. C. Apperley,
J. A. K. Howard, P. W. Dyer* **8674 – 8677**

A Truly Multifunctional Heterocycle: Iminophosphorane, N,P Chelate, and Dihydropyridine

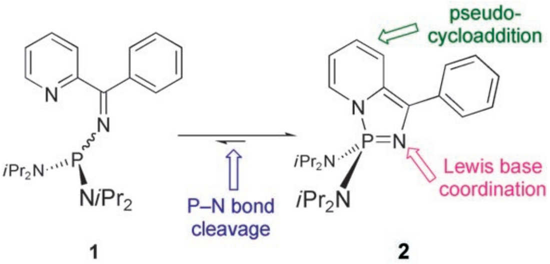

Three in one: The anellated σ^4-1λ^5-[1,3,2]diazaphosphole **2** exists in tautomeric equilibrium with isomer **1** (see scheme) and undergoes three completely different types of reaction: trimethyl aluminum binds at the N terminus of the P=N bond with ring retention, the dihydropyridine fragment reacts with an activated acetylene in a pseudo-[2+2] cycloaddition, and P–N bond cleavage is possible with Rh^I.

Sigmatropic Rearrangement

H. Kim, Y. Nguyen, A. J. Lough,
J. Chin* ______ **8678 – 8681**

Stereospecific Diaza-Cope Rearrangement Driven by Steric Strain

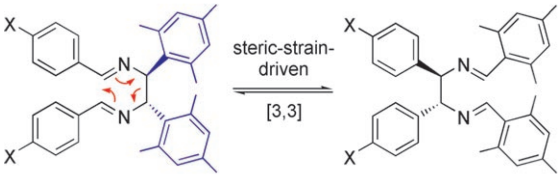

Buckling under the strain: Steric strain was used to drive the diaza-Cope rearrangement to completion (see scheme) with a high degree of stereospecificity (> 99.5 % *ee*), as evidenced by chiral-phase HPLC and crystal data. There is good agreement between the experimental and computational values for the rate and equilibrium constants for the rearrangement.

Brilliant orbs: A facile and highly efficient synthetic strategy combines evaporation-induced assembly and acetic acid mediated sol–gel chemistry for the production of various single- and multicomponent mesoporous metal oxide spheres. These spheres, which are micrometer-sized and have high surface areas and high framework crystallinity, will find many applications in catalysis and photocatalysis.

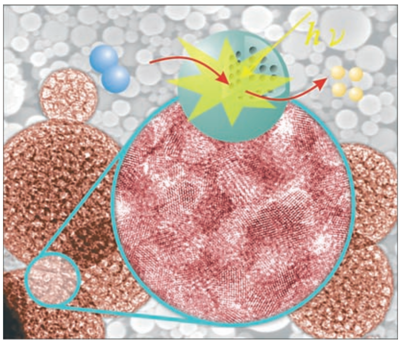

Mesoporous Materials

C.-K. Tsung, J. Fan, N. F. Zheng, Q. H. Shi, A. J. Forman, J. F. Wang,* G. D. Stucky* ———— **8682 – 8686**

A General Route to Diverse Mesoporous Metal Oxide Submicrospheres with Highly Crystalline Frameworks

---

A molecular vise: The purple-colored bis(*tert*-butylscorpionate) iron(II) complex is fully low-spin at room temperature, despite the steric hindrance brought about by the six methyl groups in the equatorial belt. The remotely situated bulky *tert*-butyl substituent on boron acts like a locking screw for a vise, forcing the tripod-shaped ligand to close, thus favoring low-spin complex formation.

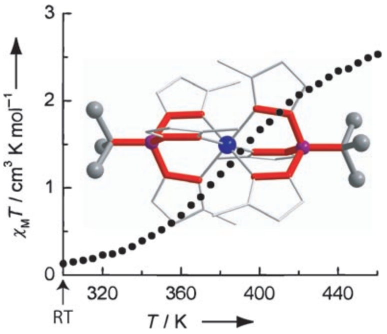

Low-Spin Iron Complex

P. Hamon, J.-Y. Thépot, M. Le Floch, M.-E. Boulon, O. Cador, S. Golhen, L. Ouahab, L. Fadel, J.-Y. Saillard, J.-R. Hamon* ———— **8687 – 8691**

Dramatic Remote Substitutent Effects on the Electronic Spin State of Bis(scorpionate) Iron(II) Complexes

---

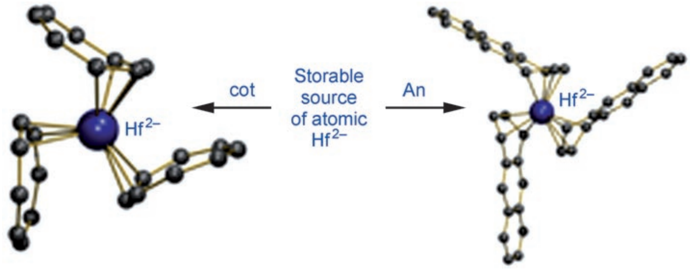

Being positive about anions: Hydrocarbon complexes containing negative-valent Hf are obtained for the first time as tris(polyarene)hafnates(2−), polyarene = anthracene (An) and naphthalene, where the latter functions as a synthon for the unknown atomic Hf^{2-} (see scheme, cot = 1,3,5,7-cyclooctatetraene). Tris(anthracene)metalates(2−) of Ti and Zr were also accessed, which completes an unprecedented triad of tris(arene)metal complexes.

Organometallic Chemistry

VIP

R. E. Jilek, M. Jang, E. D. Smolensky, J. D. Britton, J. E. Ellis* ———— **8692 – 8695**

Structurally Distinct Homoleptic Anthracene Complexes, $[M(C_{14}H_{10})_3]^{2-}$, M = Titanium, Zirconium, Hafnium: Tris(arene) Complexes for a Triad of Transition Metals

Contents

Long-Range Hydride Shift

M. Harmata,* C. Huang, P. Rooshenas, P. R. Schreiner* ———— 8696 – 8699

An Interrupted [4+3] Cycloaddition Reaction: A Hydride Shift (Ene Reaction) Intervenes

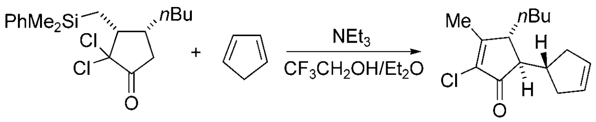

The road less traveled does indeed make all the difference. The reaction of oxyallylic cations with cyclopentadiene usually yields a [4+3] cycloadduct. Instead, a hydride shift can supersede this cycloaddition process and proceed in synthetically useful yields (see scheme). Computational analyses suggest that substantial electronic effects influence the "road" taken by the oxyallylic cation.

Asymmetric Organocatalysis (1)

C. Gianelli, L. Sambri, A. Carlone, G. Bartoli, P. Melchiorre* — 8700 – 8702

Aminocatalytic Enantioselective *anti*-Mannich Reaction of Aldehydes with In Situ Generated *N*-Cbz and *N*-Boc Imines

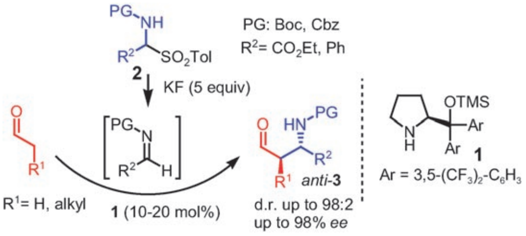

The title reaction catalyzed by the commercially available chiral secondary amine **1** proceeds with high stereocontrol and allows the in situ generation of N-carbamate-protected imines from stable α-amido sulfones **2**. This organocatalytic approach provides easy and convenient access to valuable compounds **3** in high yield, with very good *anti* selectivity, and in high enantiomeric purity.

Asymmetric Organocatalysis (2)

F. Pesciaioli, F. De Vincentiis, P. Galzerano, G. Bencivenni, G. Bartoli, A. Mazzanti, P. Melchiorre* 8703 – 8706

Organocatalytic Asymmetric Aziridination of Enones

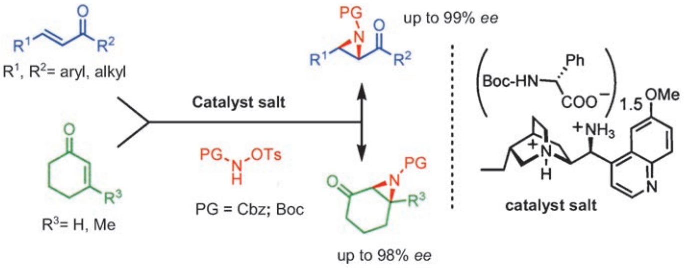

A primary amine derived from cinchona alkaloids as a salt with D-*N*-Boc phenylglycine (Boc = *tert*-butoxycarbonyl) is an efficient catalyst for the aziridination of α,β-unsaturated ketones. This method is effective with both linear and cyclic substrates, leading to chiral aziridines in high yield, with complete diastereoselectivity, and with very high enantioselectivity (Cbz = benzyloxycarbonyl).

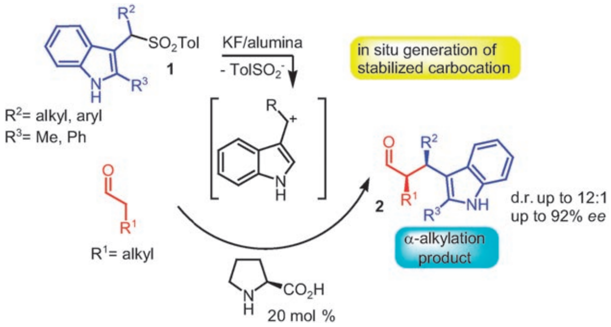

Proline strikes again: The intermolecular enamine-catalyzed asymmetric "formal" α-alkylation of aldehydes is described. Alkylating reagent **1** generates a highly stabilized carbocation, which can readily intercept the enamine intermediate. L-Proline proved to be the best catalyst, providing an easy route to relevant 3-indolyl derivatives **2** with high diastereo- and enantiocontrol.

Asymmetric Organocatalysis (3)

R. R. Shaikh, A. Mazzanti, M. Petrini,*
G. Bartoli, P. Melchiorre* ___ **8707 – 8710**

Proline-Catalyzed Asymmetric Formal α-Alkylation of Aldehydes via Vinylogous Iminium Ion Intermediates Generated from Arylsulfonyl Indoles

---

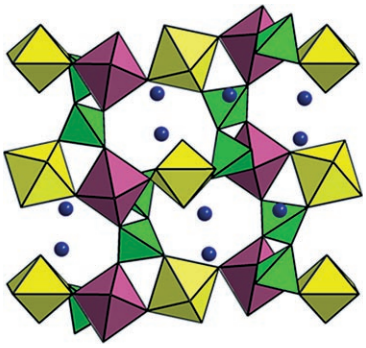

An unusual mix: The first mixed-valence uranium(V,VI) germanates are synthesized under hydrothermal conditions. The structure of $A_3(U_2O_4)(Ge_2O_7)$ (A = Rb, Cs) contains chains of corner-sharing $U^{5+}O_6$ octahedra (purple) and $U^{6+}O_6$ tetragonal bipyramids (yellow), which are interconnected by GeO_4 tetrahedra (green) to form a 3D framework (see picture; A blue).

Hydrothermal Synthesis

C.-H. Lin, K.-H. Lii* ___ **8711 – 8713**

$A_3(U_2O_4)(Ge_2O_7)$ (A = Rb, Cs): Mixed-Valence Uranium(V,VI) Germanates

---

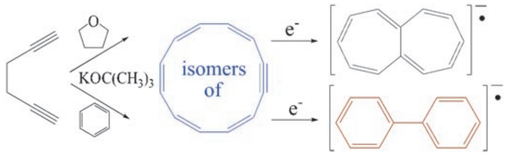

[12]Annulyne not like benzyne: The base-initiated condensation of hexadiyne in nonpolar solvents leads directly to the symmetrical isomers of [12]annulyne, i.e. the all *cis* isomer, which exists as its cumulene, and the 6,9-*trans*,*trans* isomer. One-electron transfer to this mixture leads to the formation of an unsymmetrical [12]annulyne radical anion, which transfers an electron to the all *cis* system leading to the biphenyl radical anion, while reduction of the other isomer leads to heptalene (see scheme).

Antiaromatic Rings

B. D. Rose, R. C. Reiter,
C. D. Stevenson* ___ **8714 – 8718**

The Isomers of [12]Annulyne and their Reactive Relationships to Heptalene and Biphenyl

---

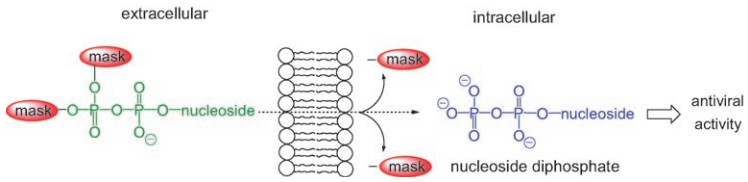

Going incognito: A new prodrug approach has been developed to facilitate the diffusion of highly polar polyphosphorylated nucleosides across cell membranes (see scheme). Inside the cell, the masking groups on the nucleoside diphosphate should be cleaved rapidly by enzymes to release the antiviral active cargo.

Nucleoside Diphosphate Prodrugs

H. J. Jessen, T. Schulz, J. Balzarini,
C. Meier* ___ **8719 – 8722**

Bioreversible Protection of Nucleoside Diphosphates

Contents

Organocatalysis

S. Lakhdar, T. Tokuyasu,
H. Mayr* ________ **8723 – 8726**

Electrophilic Reactivities of α,β-Unsaturated Iminium Ions

How fast do nucleophiles add to iminium ions? Kinetic studies of the reactions of seven iminium ions **1** with cyclic ketene acetals **2** rendered electrophilicity parameters *E* for these iminium ions. Because *N* and *s* parameters are known for numerous nucleophiles, the correlation $\log k(20\,°\mathrm{C}) = s(N+E)$ makes it possible to calculate rate constants for nucleophilic attack at the iminium ions **1**.

Aldehyde Oxidation

J. Guin, S. De Sarkar, S. Grimme,
A. Studer* ________ **8727 – 8730**

Biomimetic Carbene-Catalyzed Oxidations of Aldehydes Using TEMPO

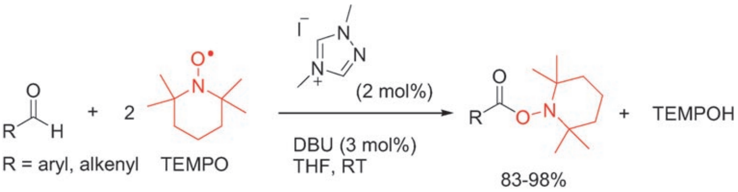

Transition-metal-free organocatalytic oxidations of various aldehydes proceed with the TEMPO radical as a mild organic oxidant; the resulting TEMPO esters are formed in moderate to excellent yields (see scheme). N-Heterocyclic carbenes (NHCs) are efficient catalysts and activate aldehydes for electron-transfer reactions. The TEMPO esters are readily hydrolyzed and the nitroxide can be regenerated by aerobic oxidation.

Infrared Spectroscopy

K. Fumino, A. Wulf,
R. Ludwig* ________ **8731 – 8734**

Strong, Localized, and Directional Hydrogen Bonds Fluidize Ionic Liquids

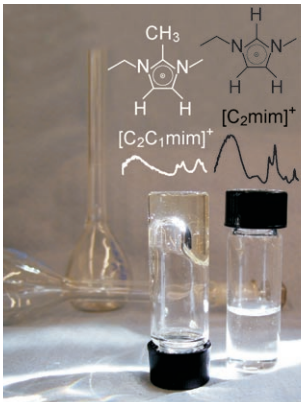

Opposite effect of hydrogen bonding: Whereas molecular liquids are stabilized, ionic liquids can be fluidized by hydrogen bonds. Highly directional H bonds introduce "defects" into the Coulomb network resulting in reduced melting points and decreased viscosities. This is shown by the mid- and far-FTIR spectra of two ionic liquids. (Structure in black: all H bonds are possible, structure in white: methyl group prevents one H bond.)

Superoxide Dismutase Mimics

M. R. Filipović, K. Duerr,
M. Mojović, V. Simeunović,
R. Zimmermann, V. Niketić,*
I. Ivanović-Burmazović* ________ **8735 – 8739**

NO Dismutase Activity of Seven-Coordinate Manganese(II) Pentaazamacrocyclic Complexes

Redox selectivity? Seven-coordinate manganese(II) pentaazamacrocyclic complexes stimulate NO disproportionation by a novel dismutation mechanism based on the formation of labile metal–nitrosyl adducts and which is associated with the $\mathrm{Mn^{II}/Mn^{III}}$ redox cycle. The metal-bound NO in these aducts has the character and reactivity of NO^- and NO^+ species.
Ex vivo studies suggest that superoxide dismutase mimics of this kind could interfere with NO-mediated processes in biological milieu.

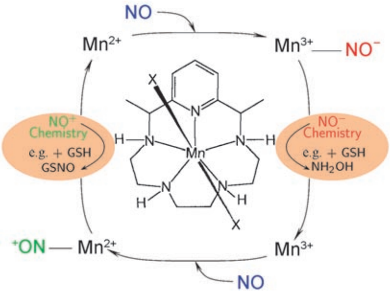

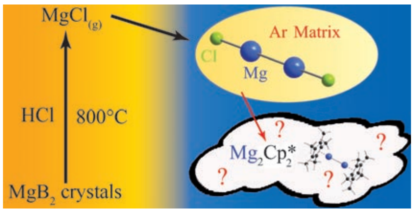

Happy together: When HCl is passed over heated MgB_2, the magnesium subhalide MgCl is formed, which converts into the dimeric linear Mg–Mg species Mg_2Cl_2 upon matrix isolation. The two compounds were characterized by vibrational spectroscopy and by computations; special attention was given to the Mg–Mg bond. The results are compared to recent findings concerning ligand-stabilized Mg–Mg species.

Mg–Mg Bonds

Supporting information is available on www.angewandte.org (see article for access details).

A video clip is available as Supporting Information on www.angewandte.org (see article for access details).

Service